

# Planar fluorescence imaging using normalized data

Vasilis Ntziachristos

Gordon Turner

Joshua Dunham

Stephen Windsor

Antoine Soubret

Jorge Ripoll

Helen A. Shih

Massachusetts General Hospital & Harvard Medical School

Center for Molecular Imaging Research  
Laboratory for Biooptics and Molecular Imaging  
Charlestown, Massachusetts 02129  
E-mail: vasilis@helix.mgh.harvard.edu

**Abstract.** Fluorescence imaging of tissues has gained significant attention in recent years due to the emergence of appropriate reporter technologies that enable noninvasive sensing of molecular function *in vivo*. Two major approaches have been used so far for fluorescence molecular imaging, i.e., epi-illumination (reflectance) imaging and fluorescence molecular tomography. Transillumination is an alternative approach that has been employed for imaging tissues in the past and could be similarly beneficial for fluorescence molecular imaging. We investigate data normalization schemes in reflectance and transillumination mode and experimentally demonstrate that normalized transillumination offers significant advantages over planar reflectance imaging and over nonnormalized methods. Our observations, based on phantoms and on postmortem and *in vivo* mouse measurements display image quality improvement, superior depth sensitivity, and improved imaging accuracy over the nonnormalized methods examined. Normalized planar imaging retains implementation simplicity and could be used to improve on standard fluorescence reflectance imaging and as a simplified alternative to the more integrated and accurate tomographic methods. © 2005 Society of Photo-Optical Instrumentation Engineers. [DOI: 10.1117/1.2136148]

Keywords: transillumination; light scattering; optical imaging; molecular imaging; diffusion.

Paper 05007RRR received Jan. 11, 2005; revised manuscript received Jul. 19, 2005; accepted for publication Jul. 21, 2005; published online Dec. 20, 2005.

## 1 Introduction

Fluorescence imaging has recently emerged as an important method for *in vivo* imaging of gene expression and protein function in live tissues. Subsequently, its application to small animal research has intensified due to the availability of an increasing number of animal models and fluorescent reporter technologies.<sup>1-4</sup> Light has been traditionally used for high-resolution imaging of histological slices using fluorescence microscopy and for tissue sectioning with confocal and multiphoton microscopy.<sup>5,6</sup> In these investigations, light in the visible spectral region is traditionally used. For probing deeper in tissue, fluorochromes that emit in the near IR are employed.<sup>4</sup> This is because tissue penetration of several centimeters can be achieved in this spectral region due to low tissue absorption. Imaging in the near IR has led to a new family of optical imaging techniques that are low resolution but lead to significantly higher penetration depths and retain high molecular specificity.<sup>7</sup>

There are two major techniques that are currently considered<sup>8</sup> for fluorescence imaging, i.e., epi-illumination imaging, also termed fluorescence reflectance imaging (FRI), and fluorescence molecular tomography (FMT). FRI is technologically and methodologically a simple technique. Typically light is expanded onto the tissue surface and any back-emitted fluorescence light is captured with a highly sensitive

CCD camera.<sup>9,10</sup> This is essentially a low-light photography technique using appropriate filters and it can record mostly superficial fluorescence activity. On the other side, fluorescence tomography is being considered as a more integrated and accurate approach compared to planar imaging.<sup>11,12</sup> Major advantages include the ability for quantification, 3-D imaging and depth retrieval, higher sensitivity, and higher resolution compared to planar imaging. Tomography has been recently used *in vivo* to resolve enzyme activity<sup>12</sup> and probe treatment response to drugs<sup>13</sup> and has demonstrated superior imaging performance to FRI. Conversely, tomography is technologically more complex than planar imaging because it requires advanced instrumentation, multiple points of illumination (projections), appropriate theoretical methods for modeling photon propagation into tissues, and correspondingly efficient inversion techniques for image reconstruction.

A third imaging alternative, fluorescence transillumination, has recently appeared in dental research<sup>14</sup> and in imaging cardiac muscle activity.<sup>15</sup> The technique shines light through tissue and collects fluorescence light emitted on the other side using appropriate filters. Both reflectance and transillumination imaging can be considered as “planar imaging” techniques and can be implemented using similar components but different geometry; in reflectance, the source and the detector reside on the same side of tissue, whereas in transillumination the tissue is placed between the source and the detector. Fluorescence transillumination bears great similarity to standard transillumination used as early as in 1929 by Cutler<sup>16</sup> to spa-

Address all correspondence to Vasilis Ntziachristos, Radiology Dept., Massachusetts General Hospital, 149 13th St. Rm. 5404, Charlestown, MA 02129. Tel: 617-726-6091. Fax: 617-726-5708. E-mail: vasilis@helix.mgh.harvard.edu

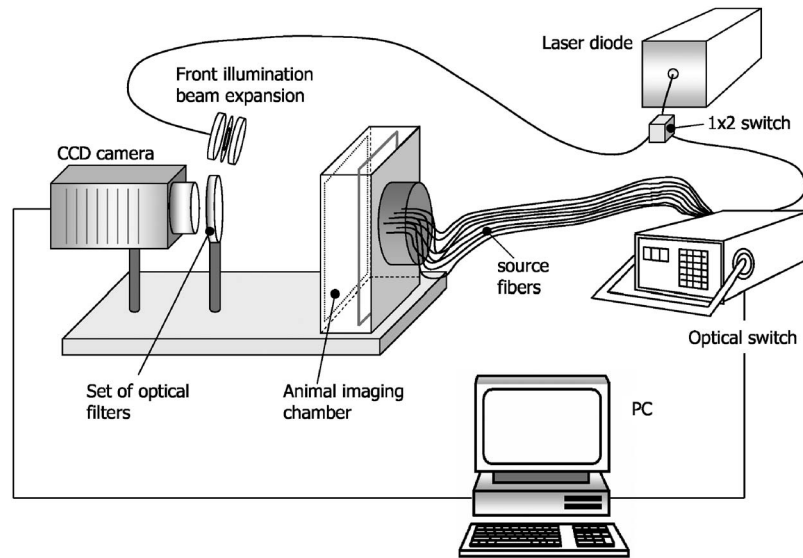


Fig. 1 Experimental setup used in the study implementing concurrent reflectance and transillumination measurements.

tially resolve absorbing lesions in the human breast. This method, known to produce “shadows” of vascular structures, the so-called “shadowgrams,” has been since pursued at different implementations, primarily for breast imaging, by several groups.<sup>17–19</sup>

Herein we investigate the merits of using normalization methods for planar imaging as alternative methods for fluorescence imaging. Normalization of fluorescence measurements using corresponding measurements at the emission wavelength was found to offer significant advantages in fluorescence tomography.<sup>20</sup> In contrast, normalized methods for planar imaging have not yet been fully explored. We therefore investigated the performance of normalized planar reflectance and normalized transillumination imaging over their nonnormalized counterparts using experimental measurements on phantoms, postmortem on animals and *in vivo*. We demonstrate, using experimental measurements from phantoms and from postmortem and *in vivo* mouse measurements, that normalized methods offer imaging performance superior to standard FRI for small animal imaging. In the following, Sec. 2 describes the experimental methods followed in this work and Sec. 3 shows key findings of our studies. The results and major implications of these studies and their application potential compared to FMT are summarized and discussed in Sec. 4.

## 2 Methods

### 2.1 Experimental Setup

To examine planar reflectance and transillumination measurements we employed a scanner similar to the one previously described for small animal tomography operating<sup>13,21</sup> in the near IR (NIR). A schematic of the system implementing planar geometry is shown in Fig. 1. Illumination was provided by a 672-nm cw laser diode (B&W Tek Newark, Delaware) with adjustable light power reaching a maximum of 100 mW, although typical powers employed in all experiments ranged within 0.5 to 2 mW. Laser light is routed through a 1×2

optical switch (Dicon Fiberoptics Inc., Richmond, California) either to beam expanding optics for reflectance imaging (front illumination) or to a programmable optical switch (Dicon Fiberoptics Inc. Richmond, California) for transillumination. The switch can time-share the light input to 46 source fibers (100/140  $\mu\text{m}$  core/clad multimode fibers). Animals are positioned into the imaging chamber that is shown in more detail in Fig. 2. The chamber is made water tight and it utilizes a front glass window that is antireflection coated for the NIR and a moving plate that can gently compress the animal against the glass window while placing the 46 source fibers onto the opposite of the animal-window interface, as shown in Fig. 2. Typical separations between the moving plate and the glass window were 1.3 cm, which is typical for small animal imaging. The 46 source fibers are evenly distributed over a field of view of  $1.8 \times 1.5$  cm onto the moving plate. Light is collected through the glass window with a CCD camera (D) ( $512 \times 512$  pixels back-illuminated VersArray from Roper Scientific/Princeton Instruments, Trenton, New Jersey) using a 35-mm  $f1.2$  lenses (Nikon Inc., Melville, New York) and bandpass filters for emission and excitation measurements ( $705 \pm 5$  and  $671 \pm 5$  nm central wavelengths, respectively, Andover Inc., Salem, New Hampshire).

### 2.2 Planar Imaging and Transillumination

The implementation of planar reflectance and transillumination geometries is illustrated in Fig. 2. Planar reflectance imaging is realized by front illuminating the imaging chamber through the glass window. Back-emitted intrinsic or excitation light is then captured by the CCD camera, which is focused on the inside surface of the glass window.

Transillumination can be implemented in several different ways. In this work, transillumination is accomplished by superposition of the signals collected through the diffuse medium imaged due to the 46 point sources at the back side of the chamber. This selection of back-illumination using superposition of point sources was herein directed by the concur-

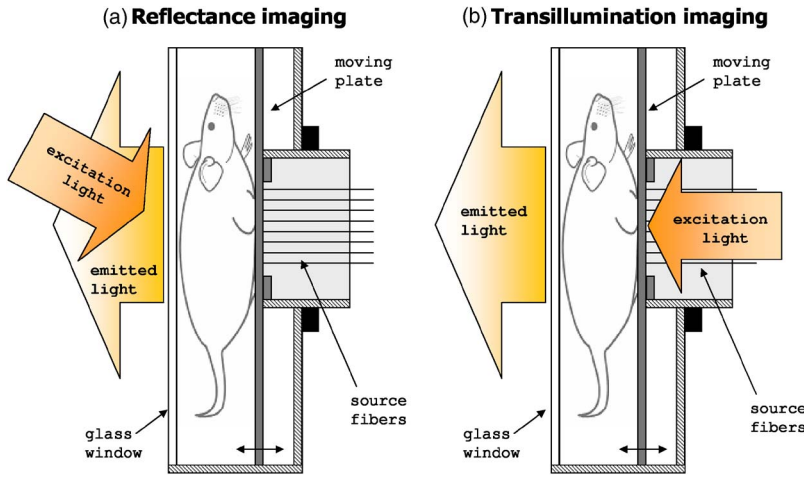


**Fig. 2** Implementation of reflectance and transillumination in the imaging chamber. (a) In reflectance mode, a beam of light is expanded onto the animal surface and light emitted back from the animal (in excitation and emission wavelengths) is collected with the CCD camera of Fig. 1 from the same side of the animal. (b) In transillumination, a group of fibers establishes an excitation beam on one side of the animal and light emitted through the animal is collected from the other side.

rent tomographic purpose that the scanner serves. Potentially, other patterns could be employed, including expanded light beams similar to reflectance imaging.

### 2.3 Measurements

We investigated normalized measurement methods and compared them to standard uncorrected signals. Typically, six images were obtained for each experiment, i.e., the front-illuminated fluorescence image (reflectance image), the back-illuminated image (transillumination), and the dark current image (noise) at both the excitation (intrinsic) and emission (fluorescence) wavelengths. We then observed the nonnormalized reflectance fluorescence image  $I_r$ , i.e.,

$$I_r = I_{fr} - I_{fn}, \quad (1)$$

where  $I_{fr}$  is the fluorescence image in reflectance mode, and  $I_{fn}$  is the background camera noise image, respectively. We acquired  $I_{fn}$  with identical acquisition and experimental parameters as  $I_{fr}$ , but in the absence of excitation light. Similarly, the transillumination fluorescence image  $I_t$  was formed as

$$I_t = \sum_{k=1}^{N_s} g(k)[I_{ft}(k) - I_{fn}]_{>T_f}, \quad (2)$$

where  $N_s$  is the number of back-illuminating sources employed,  $I_{ft}(k)$  is the transillumination fluorescence image obtained with the  $k$ 'th source on, and  $I_{fn}$  is the corresponding noise image obtained under identical conditions with no light source on. All image values above a threshold  $T_f$  are summed together to yield the transillumination image considered in our results. The threshold  $T_f$  was set at 10 times the standard deviation of the photon counts seen on  $I_{fn}$  and prevents signals of low SNR from being added up in the image  $I_t$ . Threshold  $T_f$  was of the order of 30 CCD pixel counts in the measurements presented here. The factor  $g(k)$  is a percentage coefficient that is included to correct for the variation of indi-

vidual source strengths compared to the median source strength, as calculated based on the relative strength of each source seen on corresponding measurements through homogeneous diffuse media. Note that in all cases, object illumination was provided from a common light source tuned at the fluorochrome's excitation wavelength.

Subsequently, we also examined the corresponding images after normalization with the intrinsic images acquired. The corresponding normalized reflectance image  $U_r$  can be written as

$$U_r = \frac{I_{fr} - I_{fn}}{(I_{er} - I_{en})_{>T_e}}, \quad (3)$$

where  $I_{er}$  is the reflectance imaging obtained at the emission wavelength (intrinsic image), and  $I_{en}$  is the camera noise obtained with no illumination on for the acquisition parameters used for  $I_{er}$ . We set  $U_r$  to zero unless the denominator values are above a threshold  $T_e$ , typically set to 20 standard deviations of the noise seen in  $I_{en}$  (approximately 60 photon counts). Typical  $I_{er}$  counts are in the thousands, therefore this threshold sets a very moderate noise threshold to avoid divisions with very small, noise affected values.

Similarly, the corresponding normalized transillumination image  $U_t$  can be written as

$$U_t = \frac{\sum_{k=1}^{N_s} g(k)[I_{ft}(k) - I_{fn}]_{>T_f}}{\sum_{k=1}^{N_s} g(k)[I_{et}(k) - I_{en}]_{>T_e}}, \quad (4)$$

where fluorescence and emission transillumination images for each of the  $N_s$  sources employed are summed up after subtraction with the noise images  $I_{fn}$  and  $I_{en}$  and application of the  $T_f$  and  $T_e$ , thresholds, respectively.

### 2.4 Phantoms

Two sets of phantoms were used. The first employed a relatively spatially homogeneous phantom containing two diffu-

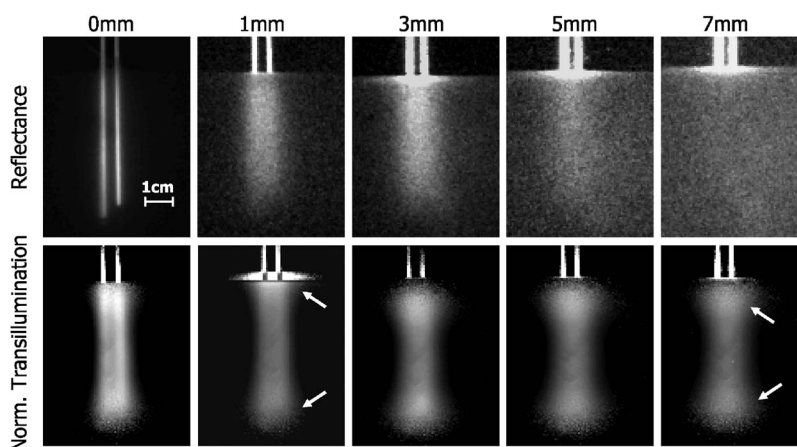


**Fig. 3** Reflectance and normalized transillumination performance as a function of depth. Top row: Reflectance images acquired with two fluorescence tubes placed at different depths as indicated on the figure titles. Bottom row: Corresponding normalized transillumination images of the same tubes and depths examined.

sive and fluorescent tubes placed 5 mm apart and immersed in a highly scattered fluid contained in the chamber. The tubes were glass capillaries of  $\sim 1.5$  mm diameter, sealed on one end, and contained a 1% intralipid solution, 25 ppm of India ink, and 200 nM of Cy 5.5 dye. The chamber was filled with the same solution of intralipid and ink, but without the fluorochrome. Subsequently, the two-tube phantom was placed at different depths in the imaging chamber to assess the relative performance of the techniques employed as a function of depth.

The second phantom examined the performance of the planar method examined to image two fluorescent tubes at varying background optical properties. These measurements employed a similar, relatively homogenous background medium, which contained two 3-mm-diam plastic tubes placed in contact with the chamber window. Both tubes and the imaging chamber contained with the same solution of 1% intralipid solution and 25 ppm amount of India ink that gives light attenuation similar to that of mouse boundaries, as determined experimentally in other studies.<sup>21</sup> The absorption coefficient of the fluid was  $\mu_a = 0.3 \text{ cm}^{-1}$  and the reduced scattering coefficient  $\mu'_s = 10 \text{ cm}^{-1}$ . In addition, the left tube contained 400 nM of Cy 5.5, whereas the right tube contained 200 nM of Cy 5.5. After this phantom was imaged, the absorption of the left tube was increased by adding India ink at  $2.5\times$  the original concentration and one imaging session was again performed. This experiment is similar to a previously reported study that assessed the tomographic performance under such conditions.<sup>13</sup>

## 2.5 Animal Imaging

Two sets of animal measurements were employed to showcase the relative merits of the techniques examined.

The first animal model consisted of a euthanized nude mouse with a 1.8-mm-diam glass tube inserted into the esophagus. The tube was filled with 1% intralipid and 400 nM of Cy5.5 dye and was positioned at the level of the midtorso of the animal. The second *in vivo* model was an MMTV/neu transgenic mouse, which exhibits multifocal spontaneous mammary tumorigenesis [FVB/N-

TgN(MMTVneu)202Mul]. An MMTV/neu mouse with two spontaneous mammary tumors was injected with 2 nmol of the cathepsin-sensitive activatable fluorescent probe ProSense680 (Visen Medical Inc., Woburn, Massachusetts).

## 3 Results

### 3.1 Imaging Performance as a Function of Depth

Figure 3 shows the measurements collected for the two fluorescent capillaries placed at different depths. The top row shows fluorescence images obtained in reflectance mode when the tubes were 0, 1, 3, 5, and 7 mm away from the front glass window. At 0 mm, the tubes are fully immersed in the diffusive fluid and physically in contact with the glass window facing the CCD camera. At larger depths, the tubes move away from the camera and the glass window into the diffusive fluid, therefore coming closer to the transillumination sources. The bottom row shows corresponding images obtained in normalized transillumination mode. We note that in Fig. 3, plain reflectance images (not normalized) are shown. This is because the intrinsic normalized reflectance images cannot record the tubes at most depths and they see only the excitation field reflected off the diffuse surface. Therefore, they do not offer correction for deep-seated activity. All images are scaled to their maximum, since signal intensity drops exponentially with depth.

The tubes are detected well in all normalized transillumination images, although resolution significantly deteriorates as a function of depth. Conversely, reflectance imaging resolves the tubes better at 0 mm than transillumination, but tube detection is overall more challenging as a function of depth. Within a millimeter away from the front window, both methods fail to resolve the two tubes. In addition, there is a characteristic broadening of the tubes, as seen in the transillumination images when moving away from the center where the sources are concentrated, as indicated by the white arrows on the 1- and 7-mm transillumination images.

This performance of transillumination imaging and key features of the normalization process are better explained in Fig. 4. Shown in Fig. 4(a) is the intrinsic field collected in

transillumination mode [ $I_{et}$  in Eq. (4)]. The field seen maps an elliptical area of  $\sim 3 \times 2$  cm on the front window and its intensity exponentially drops outside this area. Figure 4(b) shows the fluorescence image collected with the tubes of Fig. 3 at a 5-mm depth in transillumination mode. This is the nonnormalized image  $I_f$  of Eq. (2). Figure 4(c) is the normalized fluorescence image  $U_f$  described by Eq. (4), which better reveals the full length of the tubes compared to Fig. 4(b), beyond the limited area covered homogeneously by the intrinsic field. In principle, one would aim to homogeneously illuminate the complete region of interest, however, this finding indicates how the normalized method works well even at inhomogeneous back-illumination. However, due to the asymmetry of the illumination field, there is an asymmetry at the “shape” resolved at the extremes of the image (indicated with the arrows in Fig. 3).

### 3.2 Imaging Performance as a Function of Optical Property Variation

Figure 5 depicts the relative performance of normalized reflectance and transillumination for varying background optical properties. This experiment imaged the two 3-mm-diam tubes immersed in the chamber and placed in contact with the glass window facing the CCD camera. The two tubes and surrounding diffusive fluid are evident in Figs. 5(a) and 5(g), which were collected at the excitation wavelength. The left tube further contained 400 nM and the right tube 200 nM of Cy5.5, as described in the methods section.

When imaged in reflectance and transillumination both tubes demonstrated a 2:1 ( $\pm 5\%$ ) ratio in average photon counts between left and right tubes, as calculated over identical regions of interest. Subsequently, India ink was added to the left tube at a concentration of 2.5 times the background concentration. The imaging results, collected after the ink titration, are shown in Figs. 5(g)–5(l). The reflectance and transillumination measurements fail now to accurately report the 2:1 ratio of the fluorochrome concentration present in the tubes, because light is more absorbed in the left tube com-

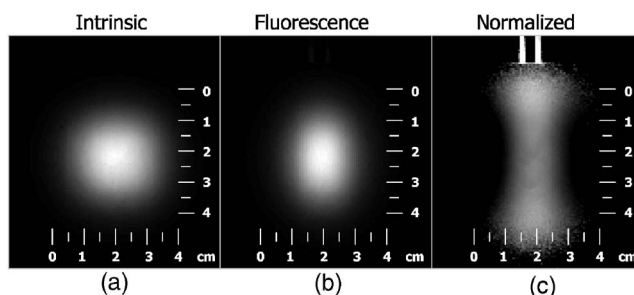


**Fig. 4** Characteristic field involved in normalized transillumination images. The intrinsic image is acquired at the excitation wavelength and the fluorescence image is the corresponding image acquired at the emission wavelength for two fluorescence tubes at 5 mm away from the front window. The normalized image, formed according to Eq. (4) described in the text, better outlines the extent of the tubes even outside the homogeneous span of the intrinsic field.

pared to the right tube due to the added absorber. The ratio’s obtained for the four fluorescence imaging approaches are summarized on the corresponding images on the text boxes in Figs. 5(h)–5(j) and 5(l).

The normalized transillumination image [Fig. 5(l)] shows the most accurate result yielding a ratio of 1.58:1 followed by normalized reflectance at 1.41:1 [Fig. 5(i)]. The worst performance (1.11:1) is seen by standard transillumination [Fig. 5(k)], where the two tubes appear to have virtually identical fluorescence. It is characteristic that even though the absorption change of the left tube is not as evident on the reflectance excitation image as it is on the excitation transillumination image (due to the white plastic tube encasing), it can nevertheless improve the quantification performance of the normalized reflectance image over the standard reflectance image. In a similar experiment,<sup>13</sup> tomography exhibited a ratio of  $\sim 1.8:1$ .

### 3.3 Small Animal Imaging

Figure 6 shows results obtained from the nude mouse implanted with a fluorescent tube after euthanasia. Figures

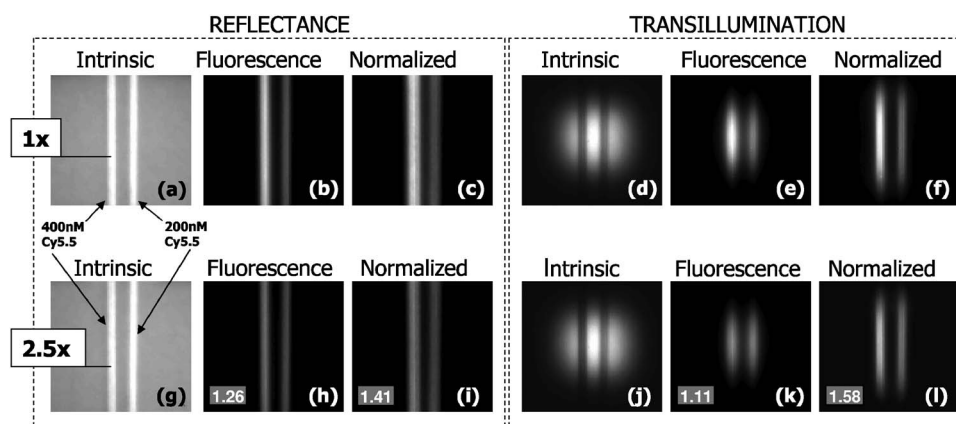


**Fig. 5** Investigation of imaging performance as a function of optical property variation. (a) to (f) Appearance of two fluorescence tubes immersed in the diffuse fluid and placed on the glass window. The left tube contains twice the fluorochrome content of the right tube (400 vs. 200 nM of the Cy5.5 fluorochrome). The optical properties in the tubes and the surrounding medium match the average optical properties of mouse boundaries in the NIR. All fluorescence imaging methods reveal correctly a 2:1 relation between fluorescence field detected from the left versus the right tube respectively. (g) to (l) Same imaging results when the absorption in the left tube is raised to 2.5 $\times$  concentration compared to the right tube. The insert text boxes report on the fluorescence strength ratio between the left and the right tubes.

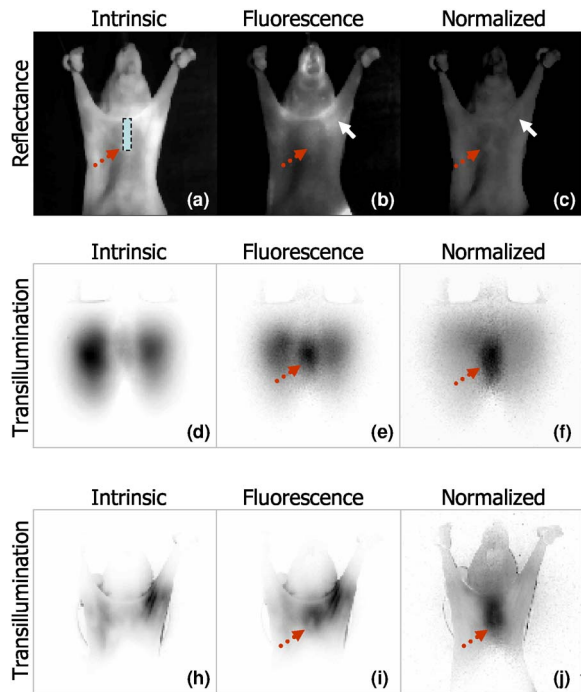


**Fig. 6** Postmortem imaging of a fluorescence tube inserted in the center of the animal through the esophagus. Top row: Intrinsic, fluorescence, and normalized reflectance images. Middle row: Intrinsic, fluorescence, and normalized transillumination images with the animal immersed in a matching diffusive medium. Bottom row: Intrinsic, fluorescence, and normalized transillumination images in the absence of a matching diffusive medium. The transillumination images are plotted in an inverse gray-scale color map. The fluorescent tube is clearly resolved in the transillumination fluorescence images as indicated by the arrows but not on the reflectance images. The best imaging performance is obtained with the normalized transillumination method.

6(a)–6(c) depict the intrinsic, fluorescence and normalized fluorescence image obtained in reflectance mode. Figure 6(a) also shows the approximate position of the tube in the viewing plane, found by measuring the insertion distance. None of the reflectance fluorescent images depict contrast from the implanted tube since, similarly to the experiment of Fig. 3, reflectance imaging is not well suited for resolving objects that are deeper than a few millimeters. Significant autofluorescence appears in Fig. 6(b), especially in the upper torso area, as indicated by the arrow. Conversely, normalization aids in obtaining a more uniform signal with less artifacts, as is apparent in Fig. 6(c), which shows lower background contrast.

Figures 6(d)–6(f), depict the intrinsic, fluorescence, and normalized transillumination images obtained in transillumination mode. Here the results are shown as negative images, i.e., darker regions indicate stronger signal. Confirming the results of Fig. 3, the tube is well detected and it is better resolved in the normalized transillumination image. The tube size is overestimated but its 2-D location is well resolved compared to its known position. While Figs. 6(d)–6(f) show results obtained at the presence of a matching fluid surrounding the animal, Figs. 6(h)–6(j) depict similar results in the absence of a matching fluid. The tube can be well observed,

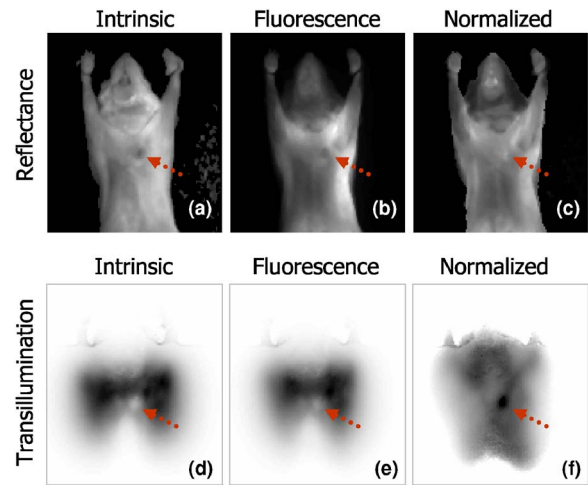


**Fig. 7** *In vivo* imaging of a subcutaneous mammary tumor. The location of the tumor is indicated by an arrow. Top row: Intrinsic, fluorescence, and normalized reflectance images. Bottom row: Intrinsic, fluorescence, and normalized reflectance images with the animal immersed in a matching diffusive medium.

and in this case, the mouse outline is also better shown. The use of matching fluids may be useful in transillumination measurements for attenuating intrinsic light close or outside the animal boundaries from directly impinging on the photon-detector and saturating the measurement. However, the absence of matching fluids offers significant experimental simplicity. In this case, special care should be taken to spatially attenuate the intrinsic light used to match the animal outline and better interface with the dynamic range of the photon detector used. In the case of Figs. 6(h)–6(j), the source distribution covered a smaller area than that covered by the animal body hence no saturation effects were observed.

Figure 7 shows an *in vivo* imaging experiment chosen from an animal bearing an ellipsoid-shaped mammary tumor of  $4 \times 3$  mm (long and short axis dimensions, respectively, as determined by caliper measurements). The tumor is indicated by an arrow in the images. This tumor was highly vascular and highly absorbing, and was therefore seen as darker than surrounding tissue on the intrinsic reflectance image shown in Fig. 7(a). The tumor, however, is not visible in the corresponding fluorescence reflectance image shown in Fig. 7(b). Similarly to the phantom results shown in Fig. 5, increased lesion absorption significantly decreases contrast in nonnormalized images. Figure 7(c) shows the normalized fluorescence reflectance image. Similarly to Fig. 6(c), this image appears to be less affected by background signals than Fig. 7(b). The tumor is also now marginally identifiable based on fluorescence signals. Overall, however, detection ability suffers mainly due to other surface fluorescence activity (autofluorescence) of comparable magnitude also observable from the animal in this case. Figures 7(d)–7(f) depict the intrinsic, fluorescence, and normalized transillumination images, also plotted in reverse scale, where a darker image indicates a stronger signal. The tumor is not visible in Fig. 7(e), and demonstrates 44% lower signal intensity compared to the stronger of background signals. However, in the normalized transillumination image shown in Fig. 7(f), the tumor can be

well seen and demonstrates a 50% fluorescence increase over the stronger of background signals as a result of the normalization method. While reflectance imaging preferentially samples surface activity, transillumination probes tumors volumetrically and yields higher detection sensitivity and contrast in this case after normalization.

#### 4 Discussion

We examined alternatives to planar reflectance imaging using a normalized reflectance approach and a normalized transillumination approach. We found that normalization attains benefits for both imaging approaches and in a variety of applications. Normalized methods were found to improve imaging performance by reducing sensitivity to the effects of optical property variation in tissues and for variations in the strength of the illumination field. Therefore, they can improve the quantification performance over conventional fluorescence reflectance imaging, especially when the background optical properties vary as is sometimes typical in *in vivo* imaging.

In addition, results show that normalized transillumination offers certain benefits when imaging deeper in tissue or volumetric responses compared to reflectance methods. This is intuitive since reflectance optical imaging is surface weighted. This means that surface features can be seen with great sensitivity but sensitivity is rapidly lost for objects that reside under the surface or deeper. This is because signal from the targeted object is exponentially attenuated with depth, while any fluorescence or autofluorescence from the surface remains recorded at full strength. By the same token, bleed-through signals, i.e., intrinsic signals detected on the fluorescence images due to imperfect filtering, are stronger in reflectance imaging since excitation light of maximum intensity is directly viewed by the CCD camera. In contrast, transillumination measurements operate on the opposite principle. Minimum excitation light is captured due to its attenuation through the diffusive volume, therefore bleed-through signals are also weak or nonexistent. Similarly, surface autofluorescence is excited by significantly attenuated light compared to reflectance approaches. Therefore, the sensitivity to tissue autofluorescence is also reduced in transillumination mode, as evinced in Figs. 6 and 7.

This study also allows for insights on the robustness of tomographic techniques as well. Transillumination measurements serve as the raw data for tomographic images. Therefore, their advantages in volume sampling, minimization of surface fluorescence, and insensitivity to the variation of optical properties carry over in the tomographic images as well. Due to the use of accurate photon propagation models and subsequent inversion, tomography can further yield 3-D quantified maps of activity and corrects for depth dependent sensitivities of photons collected. It also yields significantly higher resolution. Therefore it is a better integrated approach than either reflectance or transillumination imaging for *in vivo* imaging, but comes with added implementation complexity.

This work therefore offers an interesting alternative. Imaging performance can be improved in many cases over standard planar imaging, and therefore this method can be readily used to offer improved sensitivity to depth and improved quantification in planar imaging applications. On the other hand, normalized planar imaging is not as accurate as tomog-

raphic methods, since (1) the nonlinear dependencies of diffuse light intensity to depth are not corrected for and (2) it does not resolve depth. In addition, tomography can offer significantly more elegant methodologies to improve resolution, robustness to background heterogeneity and efficiently handle noise. This comparison of optical imaging methodologies reminds us of the technologically simple x-ray imaging versus the more involved x-ray computed tomography (CT). We envision similar utility for these methods, where certain applications, especially if lesion depth is not varied, may use normalized planar methods as stand-alone imaging methods, whereas other applications will require the added performance and accuracy of tomography. We have further found normalized transillumination measurements useful in quickly evaluating whether contrast exists in the animal or phantom imaged before applying tomographic analysis. Therefore, the proposed set of methods can be used to improve small animal imaging research and perhaps in clinical applications as well with moderate hardware and methodological improvements compared to the standard fluorescence reflectance imaging that is widely used today.

#### Acknowledgments

This work was supported in part by the U.S. Army W81XWH-04-01-239 and National Cancer Institute/National Aeronautics and Space Administration (NCI/NASA) grant No. BAA NO1-CO-17016-32.

#### References

1. R. G. Blasberg, "In vivo molecular-genetic imaging: multi-modality nuclear and optical combinations," *Nucl. Med. Biol.* **30**, 879–888 (2003).
2. T. F. Budinger, D. A. Benaron, and A. P. Koretsky, "Imaging transgenic animals," *Annu. Rev. Biomed. Eng.* **1**, 611–648 (1999).
3. D. Piwnicka-Worms, D. P. Schuster, and J. R. Garbow, "Molecular imaging of hostpathogen interactions in intact small animals," *Cell. Microbiol.* **6**, 319–331 (2004).
4. R. Weissleder and V. Ntziachristos, "Shedding light onto live molecular targets," *Nat. Med.* **9**, 123–128 (2003).
5. E. B. Brown, R. B. Campbell, Y. Tsuzuki, L. Xu, P. Carmeliet, D. Fukumura, and R. K. Jain, "In vivo measurement of gene expression, angiogenesis and physiological function in tumors using multiphoton laser scanning microscopy," *Nat. Med.* **7**, 864–868 (2001).
6. K. C. Pedley, "Applications of confocal and fluorescence microscopy," *Digestion* **58**(Suppl. 2), 62–68 (1997).
7. H. R. Herschman, "Molecular imaging: looking at problems, seeing solutions," *Science* **302**, 605–608 (2003).
8. V. Ntziachristos, C. Bremer, and R. Weissleder, "Fluorescence imaging with near-infrared light: new technological advances that enable *in vivo* molecular imaging," *Eur. J. Radiol.* **13**, 195–208 (2003).
9. S. Ke, X. X. Wen, M. Gurfinkel, C. Charnsangavej, S. Wallace, E. M. Sevick-Muraca, and C. Li, "Near-infrared optical imaging of epidermal growth factor receptor in breast cancer xenografts," *Cancer Res.* **63**, 7870–7875 (2003).
10. U. Mahmood, C. Tung, A. Bogdanov, and R. Weissleder, "Near infrared optical imaging system to detect tumor protease activity," *Radiology* **213**, 866–870 (1999).
11. M. J. Eppstein, D. J. Hawrysz, A. Godavarty, and E. M. Sevick-Muraca, "Three-dimensional, Bayesian image reconstruction from sparse and noisy data sets: nearinfrared fluorescence tomography," *Proc. Natl. Acad. Sci. U.S.A.* **99**, 9619–9624 (2002).
12. V. Ntziachristos, C. Tung, C. Bremer, and R. Weissleder, "Fluorescence-mediated tomography resolves protease activity *in vivo*," *Nat. Med.* **8**, 757–760 (2002).
13. V. Ntziachristos, E. Schellenberger, J. Ripoll, D. Yessayan, E. Graves, J. Bogdanov, A. L. Josephson, and R. Weissleder, "Visualization of anti-tumor treatment by means of fluorescence molecular tomography using an annexin V—Cy5.5 conjugate," *Proc. Natl. Acad. Sci. U.S.A.*

- 101**, 12294–12299 (2004).
14. W. Buchalla, A. M. Lennon, M. H. van der Veen, and G. K. Stookey, "Optimal camera and illumination angulations for detection of interproximal caries using quantitative light-induced fluorescence," *Caries Res.* **36**, 320–326 (2002).
  15. W. T. Baxter, S. F. Mironov, A. V. Zaitsev, J. Jalife, and A. M. Pertsov, "Visualizing excitation waves inside cardiac muscle using transillumination," *Biophys. J.* **80**, 516–530 (2001).
  16. M. Cutler, "Transillumination as an aid in the diagnosis of breast lesions," *Surg. Gynecol. Obstet.* **48**, 721–729 (1929).
  17. D. Grosenick, K. T. Moesta, H. Wabnitz, J. Mucke, C. Stroszczynski, R. Macdonald, P. M. Schlag, and H. Rinneberg, "Time-domain optical mammography: initial clinical results on detection and characterization of breast tumors," *Appl. Opt.* **42**, 3170–3186 (2003).
  18. M. A. Franceschini, K. T. Moesta, S. Fantini, G. Gaida, E. Gratton, H. Jess, W. W. Mantulin, M. Seeber, P. M. Schlag, and M. Kaschke, "Frequency-domain techniques enhance optical mammography: Initial clinical results," *Proc. Natl. Acad. Sci. U.S.A.* **94**, 6468–6473 (1997).
  19. P. Taroni, G. Danesini, A. Torricelli, A. Pifferi, L. Spinelli, and R. Cubeddu, "Clinical trial of time-resolved scanning optical mammography at 4 wavelengths between 683 and 975 nm," *J. Biomed. Opt.* **9**, 464–473 (2004).
  20. V. Ntziachristos and R. Weissleder, "Experimental three-dimensional fluorescence reconstruction of diffuse media using a normalized Born approximation," *Opt. Lett.* **26**, 893–895 (2001).
  21. E. Graves, J. Ripoll, R. Weissleder, and V. Ntziachristos, "A sub-millimeter resolution fluorescence molecular imaging system for small animal imaging," *Med. Phys.* **30**, 901–911 (2003).